Ab initio thermodynamics of the CoCrFeMnNi high entropy alloy: Importance of entropy contributions beyond the configurational one

Duancheng Ma [a,*], Blazej Grabowski [a,*], Fritz Körmann [b,*], Jörg Neugebauer [a], Dierk Raabe [a]

[a] Max-Planck-Institut für Eisenforschung GmbH, Max-Planck-Straße 1, 40237 Düsseldorf, Germany
[b] Department of Materials Science and Engineering, Delft University of Technology, Mekelweg 2, 2628 CD Delft, Netherlands

A B S T R A C T

We investigate the thermodynamic properties of the prototype equi-atomic high entropy alloy (HEA) CoCrFeMnNi by using finite-temperature ab initio methods. All relevant free energy contributions are considered for the hcp, fcc, and bcc structures, including electronic, vibrational, and magnetic excitations. We predict the paramagnetic fcc phase to be most stable above room temperature in agreement with experiment. The corresponding thermal expansion and bulk modulus agree likewise well with experimental measurements. A careful analysis of the underlying entropy contributions allows us to identify that the originally postulated dominance of the configurational entropy is questionable. We show that vibrational, electronic, and magnetic entropy contributions must be considered on an equal footing to reliably predict phase stabilities in HEA systems.

© 2015 Acta Materialia Inc. Published by Elsevier Ltd. All rights reserved.

1. Introduction

High entropy alloy (HEA) refers to a multi-component (5 or more) single-phase solid-solution alloy in or near an equi-atomic composition [1–3]. The basic idea behind HEAs is an exploration of phase diagrams which are not confined to regions of a single major base element as in conventional alloy design. The aim of the new concept is a development of new alloy systems with novel mechanical and functional properties [1–4]. The term "high entropy" refers to the high configurational entropy which is deemed to be responsible for the stability of the single solid solution phase over competing intermetallic and elemental phases [1,2]. The configurational entropy is however only one out of various contributions to the Gibbs free energy and it is the latter that determines phase stabilities. It is therefore of crucial importance to also investigate the role of (1) the formation enthalpy and (2) other entropy contributions.

The role of the formation enthalpy has been recently addressed by [5]. The authors showed that among various multi-component alloys with equal ideal configurational entropy only one was sufficiently stabilized to form a single-phase solid-solution. In all other multi-component alloys studied in Ref. [5], the formation enthalpy was dominant over the configurational entropy resulting in the

formation of intermetallic phases. The impact of entropy contributions other than the configurational one on the phase stability of HEAs has so far only scarcely been addressed. Rather, with reference to the first core effect, it has been implicitly assumed that entropic contributions related to atomic vibrations, electronic and magnetic excitations are negligible in determining phase stabilities in HEAs.

In the present paper we employ ab initio based simulations to investigate the validity of the latter assumption for the prototype HEA CoCrFeMnNi [6–10]. In particular, we study the phase stability between hcp, fcc, and bcc structures by calculating the free energies of the respective crystal structures at $T = 0$ K as well as at finite temperatures, including a detailed analysis of the balance between the different entropy contributions (vibrational, electronic, magnetic as well as configurational).

2. Methodology

The Gibbs energy of the CoCrFeMnNi alloy is derived by Legendre transforming the volume- and temperature-dependent free energy $F(V,T)$ computed within the adiabatic approximation according to [11,12]

$$F(V,T) = E^{0\,K}(V) + F^{el}(V,T) + F^{vib}(V,T) + F^{mag}(V,T) - TS^{conf}(T), \quad (1)$$

where E^{0K} is the $T = 0$ K total energy, F^{el}, F^{vib}, and F^{mag} are the electronic, vibrational, and magnetic free energies, respectively, and S^{conf} is the ideal configurational entropy. The $T = 0$ K energy is fitted

* Corresponding authors.
    E-mail addresses: d.ma@mpie.de (D. Ma), b.grabowski@mpie.de (B. Grabowski), f.h.w.kormann@tudelft.nl (F. Körmann).

by using the Birch–Murnaghan fit [13,14]. The electronic free energy is obtained within the framework of finite temperature density-functional-theory as detailed, e.g., in [15]. Details regarding the calculation of the vibrational and magnetic free energy contributions, and the treatment of chemical and magnetic disorder are discussed in the following subsections.

2.1. Vibrational free energy

The description of the vibrational free energy from first principles for multi-component magnetic alloys is a challenging task. Despite recent progress for the description of lattice vibrations of magnetic materials at elevated temperatures (e.g. Fe [16,17], CrN [18] and Fe-alloys [19]), the methods are not yet advanced to a stage to be feasibly and practically applied for the here considered multi-component alloys. The same applies to the class of new methods which are capable of computing highly accurate anharmonic contributions which have been recently developed and applied to pure fcc elements [20,21]. For these reasons, the vibrational free energy is in this work derived by using the Debye–Grüneisen model following the work of [22]:

$$F^{\text{vib}}(V,T) = E_D(V,T) - TS^{\text{vib}}(V,T), \tag{2}$$

with E_D and S^{vib} given by

$$E_D(V,T) = \frac{9}{8}k_B\Theta_D(V) + 3k_B T \cdot D(\text{x}), \tag{3}$$

$$S^{\text{vib}}(V,T) = 3k_B\left[\frac{4}{3}D(\text{x}) - \ln\left(1 - \exp\left(-\text{x}\right)\right)\right], \tag{4}$$

where k_B is the Boltzmann constant, $D(\text{x})$ denotes the Debye function and x is given by

$$\text{x} = \frac{\Theta_D(V)}{T}. \tag{5}$$

The Debye temperature, Θ_D, is obtained as proposed by [22] using

$$\Theta_D(V_0) = C\sqrt{\frac{r_0 B_0}{M}}, \tag{6}$$

where $C = 41.63$ is an empirical constant, M the atomic mass, and r_0 the atomic radius which is connected to the equilibrium atomic volume by $r_0 = (3V_0/4\pi)^{1/3}$. The bulk modulus B_0 is evaluated at the equilibrium atomic volume V_0.

The volume dependence of the Debye temperature is evaluated through the Grüneisen parameter, γ, [22,23]:

$$\Theta_D(V) = \Theta_D(V_0) \cdot \left(\frac{V_0}{V}\right)^{\gamma}, \tag{7}$$

where γ is the Grüneisen parameter which is obtained by [23]:

$$\gamma = -g - \frac{\partial^2 P/\partial V^2}{\partial P/\partial V} = -g + \frac{1}{2}\left(1 + B_0'\right), \tag{8}$$

where B_0' is the bulk modulus pressure derivative. The factor g is determined by the underlying approximation and can assume values of $g = 2/3$ (high temperatures) proposed by [24] or $g = 1$ (low temperatures) by [25]. We adapt in the following the value of $g = 2/3$.

2.2. Magnetic free energy

Modeling of magnetic free energies from first-principles is in general a challenging task, in particular if multi-component alloy systems are considered (for recent reviews see, e.g., [26,27]). In order to handle such a complex problem, approximations are

unavoidable. The considered HEA system in the present work is suggested to be paramagnetic by [28]. Assuming that at high T magnetic short-range order can be neglected, the magnetic free energy,

$$F^{\text{mag}}(V,T) \approx -TS^{\text{mag}}(V), \tag{9}$$

is dominated by the magnetic entropy S^{mag}.[1] In the high temperature limit, far above the Curie temperature ($T \gg T_C$), the individual magnetic moments are uncorrelated and contribute to S^{mag} in a mean field approximation (MFA) as [29,26]:

$$S^{\text{mag}}(V) = k_B\sum_{i=1}^{5}c_i \ln\left(|M_i(V)| + 1\right), \tag{10}$$

where M_i is the average magnetic moment of the species i, and c_i is its atomic concentration.

Assuming an effective, one-atomic ferromagnetic species a similar mean-field treatment for the Curie temperature, T_C, can be formulated as

$$T_C = \frac{2}{3} \times \frac{E_{\text{tot}}^{\text{DLM}} - E_{\text{tot}}^{\text{FM}}}{k_B}, \tag{11}$$

where $(E_{\text{tot}}^{\text{DLM}} - E_{\text{tot}}^{\text{FM}})$ is the difference between the ground state total energies of the disordered local moment (DLM) and the ferromagnetic (FM) state [30]. In this work the difference has been computed at the equilibrium atomic volume of the FM state. The DLM is a technique to model the paramagnetic state (see Section 2.3). Note that T_C estimated by Eq. (11) typically overestimates the experimental values [31].

2.3. Ab initio treatment

The challenge in first-principles modeling of HEAs originates from three aspects: (1) the large number of different species (i.e., usually $\geqslant 5$), (2) chemical disorder, and (3) a complicated magnetic state (i.e., paramagnetism). The widely-used supercell approach to model chemical disorder, e.g., in conjunction with special quasi-random structures (SQS) or the cluster expansion (CE) technique, is for the considered HEA computationally impractical. We therefore resort in the present work to the exact muffin-tin orbitals (EMTO) method [32–35] within the framework of density functional theory (DFT) [36,37]. The EMTO technique is an improved screened Korringa–Kohn–Rostoker approach employing large overlapping potential spheres for an accurate description of the exact single-electron potential, and the full charge density method further increases accuracy bringing it close to the accuracy of full potential total energy methods [35]. It allows to model the chemical disorder employing the coherent potential approximation (CPA) [38,39,34] within an effective 1-atomic unit cell. The screened Coulomb interactions [40,41] were set to $\alpha_{\text{scr}} = 0.796$ and $\beta_{\text{scr}} = 1.0$. For the self-consistent electronic density calculations we employed the local density approximation (LDA) while the total energy has been obtained within the generalized gradient approximation (GGA) as parametrized by Perdew–Burke–Ernzerhof (PBE) [42]. The Brillouin zone integration was done by using $40 \times 40 \times 40$ for fcc and bcc, and $40 \times 40 \times 24$ for hcp k-point mesh according to the Monkhorst–Pack scheme [43]. Three different magnetic scenarios have been considered, i.e., the non-magnetic (NM), the ferromagnetic (FM), and the paramagnetic state. The latter has been modeled employing the disordered local moment (DLM) model [44,45].

A main limitation of the employed EMTO-CPA approach is the neglect of local relaxation effects, which are related to the core

---

[1] The constant contribution of the magnetic internal energy is included into the total ground state energy.

effects in HEAs. Recent studies, however, reveal good agreement between CPA and supercell approaches for a four components HEA, i.e., CoCrFeNi [46], and deviations of the bulk modulus and the lattice parameter obtained by the supercell approach are 0.5% and 0.2% from the values by CPA, respectively. Moreover, the EMTO method has been recently successfully applied to study similar HEA systems as well [47,46,48–50].

3. Results

3.1. Ground state properties

We first focus on the stability at $T = 0$ K and in particular on the role of magnetism. Fig. 1(a) shows the total energy as a function of volume for hcp, fcc, and bcc within the three considered magnetic states, i.e., NM, FM and DLM. For clarity, the total energies are referenced with respect to the equilibrium total energy of FM bcc. We see that, independent of the magnetic state, the hcp structure is the most favorable one at zero temperature and, independent of the structure, the FM state is always the energetically lowest one. Thus, overall the FM hcp structure is predicted to be the stable phase at $T = 0$ K.

The magnetic contribution in bcc is much larger compared to hcp and fcc as indicated by the large energetic differences among the phases. In clear contrast, the energy differences in hcp are almost negligible close to the equilibrium volume. This finding is directly related to the local magnetic moments shown Fig. 1(b) and (c). Close to the equilibrium volume, the FM and DLM states of hcp have almost vanishing local magnetic moments and resemble therefore closely the NM state. At larger volumes the local magnetic moments significantly increase indicating strong magneto-
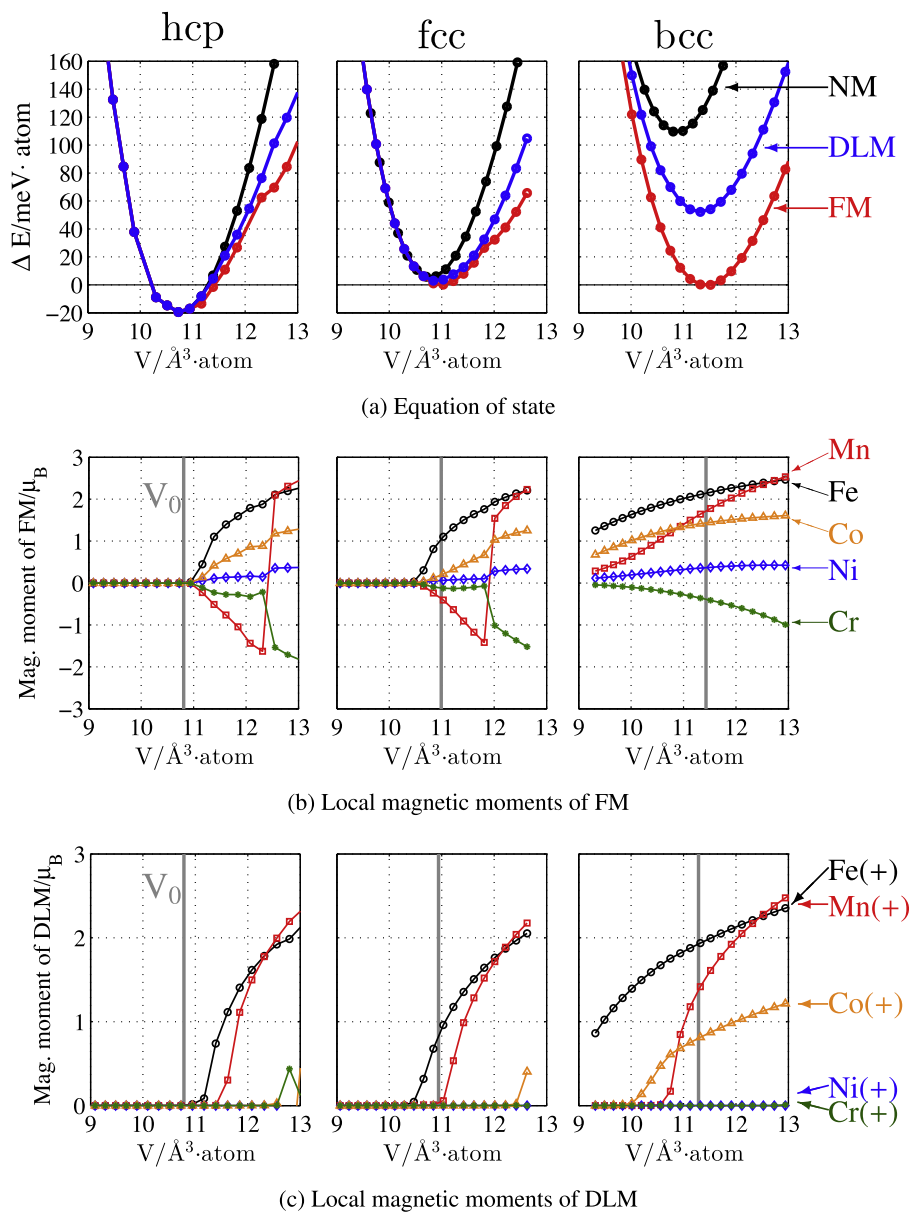

(a) Equation of state

(b) Local magnetic moments of FM

(c) Local magnetic moments of DLM

Fig. 1. (a) Ground state equation of states. Left column: hcp; middle column: fcc; right column: bcc. All total energies are referenced with respect to the total energy of bcc FM at its equilibrium volume. (b) Local moments of individual elements assuming the ferromagnetic (FM) state. (c) Local magnetic moments assuming the disordered local moments (DLM) state. Color code: in (a), black: non-magnetic (NM); red: ferromagnetic (FM); blue: disordered local moments (DLM). In (b) and (c), black open circles: Fe; red open squares: Mn; dark orange open triangles: Co; blue open diamonds: Ni; dark green solid circles: Cr. The vertical gray lines in the middle and bottom row indicate the equilibrium volume. (For interpretation of the references to color in this figure legend, the reader is referred to the web version of this article.)

volume effects. A similar phenomenon has been observed in a Fe–Mn binary solid solution in hcp for the DLM state [51]. In contrast to fcc and hcp, the local magnetic moments in the bcc structure are already significant at the ground state volume and thus strongly contribute to the phase stabilities.

Studying the magnetic properties in more detail we find that in all three considered structures, a fully ferromagnetic alignment is energetically unstable and eventually a ferrimagnetic state is predicted with Cr being always antiferromagnetically aligned to the ferromagnetic Fe, Co, and Ni. The phenomenon of Cr being antiferromagnetically aligned to Fe, Co, and Ni was also observed in a four component CoCrFeNi alloy [52]. In the hcp and fcc structure, Mn is antiferromagnetically aligned as well. We furthermore observe a magnetic transition in FM hcp and fcc with increasing volume. The direction of the magnetic moment on the Mn atoms is flipped due to a low-spin to high-spin transition on the Co, Ni, and Cr atoms, while the magnetic moment on the Fe-sites remains unaffected. This magnetic transition is also the reason for a kink in the total energy vs. volume curves of FM hcp and fcc in Fig. 1(a). For small volumes below the magnetic transition, the major magnetic moment carriers in the FM hcp and fcc structure are Fe and Mn, and they are anti-ferromagnetically aligned. For larger volumes, the volume dependence of the local magnetic moments of FM hcp and fcc becomes similar to that of bcc FM. The situation is different for bcc, where for both magnetic scenarios, FM and DLM, the major magnetic moment carriers ($> 1\mu_B$) are given by the Fe, Mn, and Co atoms, being collinearly aligned, where μ_B is a Bohr magneton.

The equilibrium lattice constant and bulk modulus shown in Fig. 2 have been extracted by fitting a Birch–Murnaghan fit [13,14] to the energy volume curves shown in Fig. 1(a). Due to the above discussed magnetic transitions in fcc and hcp for FM and DLM, in particular the bulk modulus is very sensitive to the volume range used for the fitting. We have ensured that the volumes included (see Table 1) are properly chosen to represent the physically relevant range of the corresponding magnetic state.

In general, we find V_0 to be largest in bcc, and smallest in hcp. The equilibrium volume in hcp is practically the same for all considered magnetic states due to the vanishing local moments (see above). For fcc and bcc, the largest and smallest V_0 occur for the FM and NM state, respectively. The situation is reversed if the bulk modulus, B_0, is considered. B_0 is the largest for the NM state whereas it is the smallest for the FM state. It is worth mentioning that for the NM calculations, the different B_0 and V_0 of hcp, fcc, and bcc are all very close to each other.

3.2. Phase stability at finite temperatures

In order to investigate the relative phase stability at finite temperatures, the free energies of hcp, fcc, and bcc for the three magnetic states, NM, FM, and DLM are plotted in Fig. 3 with reference to the bcc FM state. For NM, the phase ordering at finite temperature remains the same as at $T = 0$ K, i.e., hcp is the stable phase and bcc is the most unstable phase. Assuming a FM or DLM state, hcp is the stable phase below ~460 K for FM and below ~340 K for DLM, and above those temperatures fcc is the stable phase.

To assess whether the appropriate magnetic scenario is FM or DLM, the Curie temperature, T_C, has been computed according to Eq. (11). We find a small T_C for hcp and fcc of about 13 and 20 K, whereas it is much larger for the thermodynamically less preferred bcc structure (410 K). The phase stability sequence including the magnetic transition is thus predicted to be: (i) hcp FM for $T < 13$ K, hcp DLM for $13 < T < 340$ K, and fcc DLM for $T > 340$ K. The fcc DLM state is also observed in experiment. This clearly indicates the important role of magnetism in the HEA
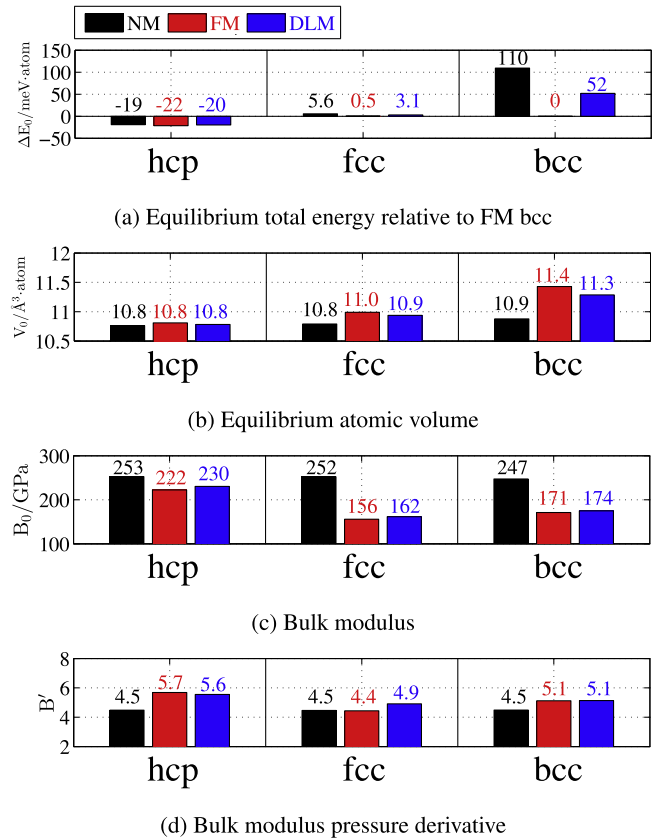

(a) Equilibrium total energy relative to FM bcc

(b) Equilibrium atomic volume

(c) Bulk modulus

(d) Bulk modulus pressure derivative

Fig. 2. Ground state properties of CoCrFeMnNi in the hcp (left), fcc (middle), and bcc (right) structure, assuming the NM (non-magnetic, black), FM (ferromagnetic, red), and DLM (disordered local moments, blue) state. The four rows show (from top to bottom) the (a) difference of the equilibrium total energies with respect to bcc FM, ΔE_0, (b) the equilibrium volume, V_0, (c) the equilibrium bulk modulus, B_0, and (d) its pressure derivative, B_0'. (For interpretation of the references to color in this figure legend, the reader is referred to the web version of this article.)

Table 1
Volume ranges, V, of the total energy vs. volume curves (Fig. 1(a)) used for the Birch–Murnangan fit [13,14], with V_0 the equilibrium volume as shown in Fig. 2(b).

hcp	FM	$0.81V_0 < V < 1.07V_0$
	DLM	$0.81V_0 < V < 1.10V_0$
fcc	FM	$0.95V_0 < V < 1.07V_0$
	DLM	$0.94V_0 < V < 1.12V_0$

considered. Without considering spontaneously spin-aligned magnetism, i.e., for the NM scenario, hcp is always the stable phase from $T = 0$ K up to 1200 K. In contrast, in the FM and DLM states, fcc becomes stable for increasing temperatures, which can be traced back to implicit and explicit magnetic contributions. Since the local magnetic moments are vanishing in hcp DLM in contrast to fcc DLM, the *explicit* magnetic entropy, Eq. (10), clearly stabilizes the fcc structure with increasing temperature.

Furthermore, the inclusion of spin-polarization decreases the bulk modulus lowering thereby the Debye temperature. This magnetically driven decrease in the Debye temperature corresponds to a softening of lattice vibrations and increases therefore the vibrational entropy in Eq. (3), see also Fig. 4. Again, since magnetism has virtually no impact on the hcp FM and DLM state due to the virtually vanishing moments, this *implicit* magnetic contribution, via the coupling of magnetism and elastic properties, is smaller
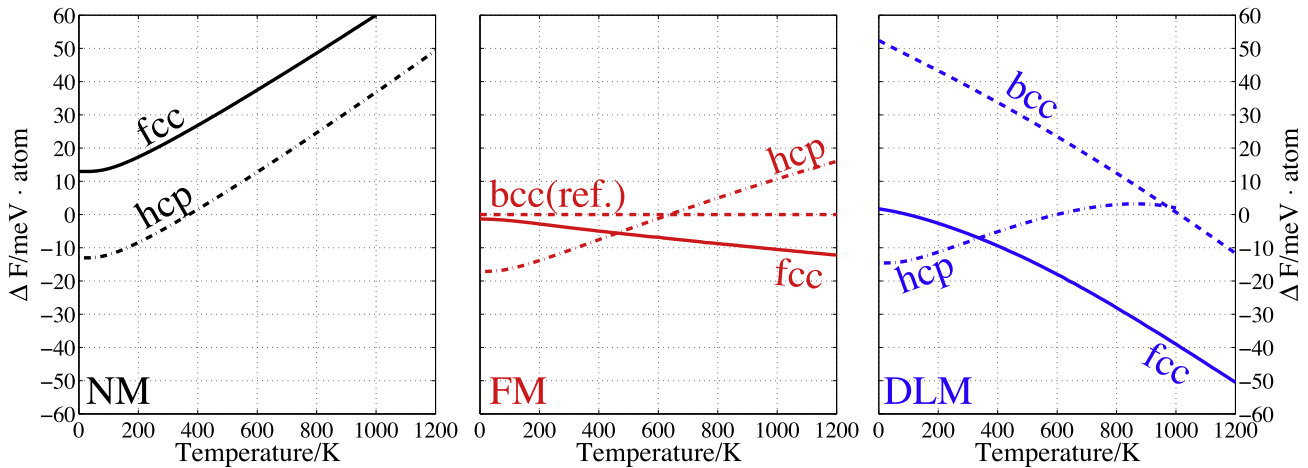
Fig. 3. Free energy curves of CoCrFeMnNi in the hcp (dash-dotted lines), fcc (solid lines), and bcc (dashed lines) structure for the NM (non-magnetic, left), FM (ferromagnetic, middle), and DLM (disordered local moments, right) state. The free energy curve of NM bcc is >110 meV/atom and thus beyond the plotted range. Above 1000 K, the hcp DLM free energies are not continued, because the equilibrium volume of hcp DLM falls beyond the range of investigated volumes. The Curie temperatures of hcp, fcc, and bcc are predicted to be 13, 20, and 410 K (see Eq. (11)).
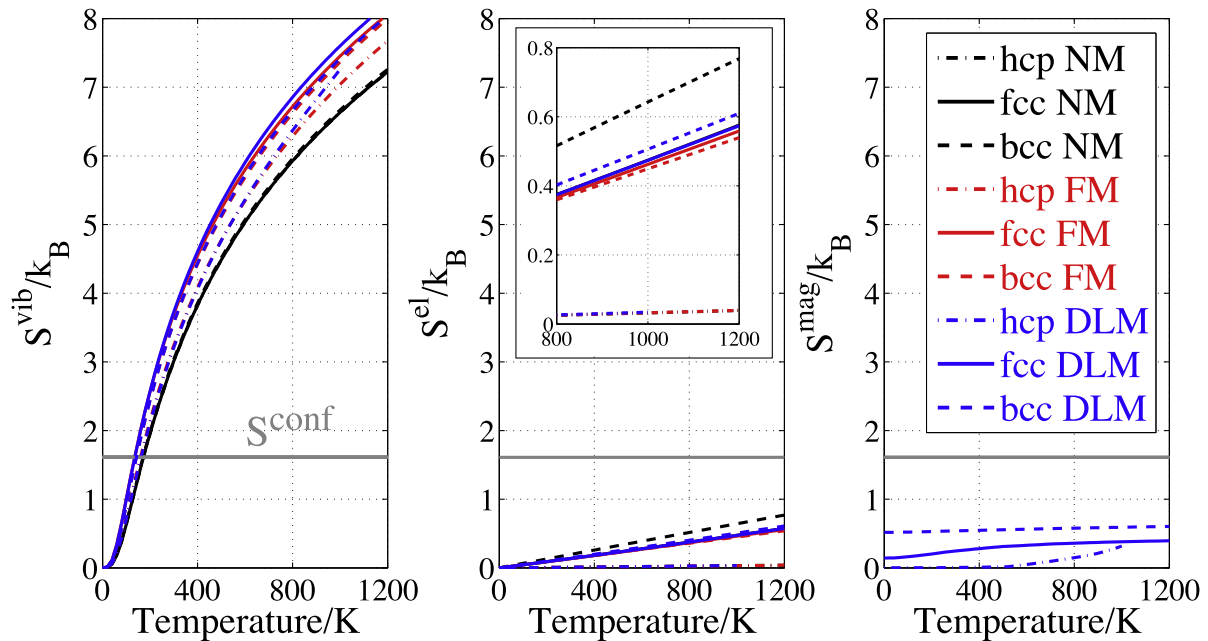

Fig. 4. Temperature dependence of the vibrational entropy S^{vib} (left), the electronic entropy S^{el} (middle), and the magnetic entropy S^{mag} (right) in the hcp (dash-dotted lines), fcc (solid lines), and bcc (dashed lines) structure for the NM (black), FM (red), and DLM (blue) state. Gray horizontal lines indicate the configurational entropy S^{conf}. (For interpretation of the references to color in this figure legend, the reader is referred to the web version of this article.)

for hcp than for fcc (see Fig. 2)). Altogether we, however, still obtain a hcp structure at low temperatures.

An hcp structure has not been observed so far, neither at room temperature [8,5,53,54] nor at cryogenic temperatures down to 77 K [55,56]. However, twinning induced plasticity (TWIP) has been observed in the investigated HEA at cryogenic temperatures (77 K) [55,56]. This indicates that the hcp phase is energetically very close to the fcc phase.

The non-existence of the hcp phase in experiment might be a result of kinetic limitations of the phase transformation under experimental conditions. The free energies shown in Fig. 3 relate to the thermodynamic ground state only. From a kinetic perspective, the transformation from fcc to hcp depends on the entire γ-surface [57]. We suspect that the γ-surface for the here

investigated HEA alloy is complex and kinetically hinders the transformation to hcp.

Note that despite the consistency between the theoretical prediction achieved in this study and experimental observations [5–10] (i.e., fcc DLM state is more stable than hcp and bcc), it has been revealed by simulations [58] and experiments [59,60] that at low temperatures phase separation can occur. Annealing at an intermediate temperature, e.g., below ~870 K, precipitates, such as a Mn–Ni phase, a Cr-rich phase, and a Fe–Co phase, have been observed [58,60]. This is not in contradiction to our study in which these competing phases and phase separation are not considered. The here investigated fcc single-phase solid solution is stable at higher temperatures (~870 K) and might be retained by fast cooling [58,61].

3.3. Entropy contributions due to different excitations

Figure 4 shows the different entropy contributions (vibrational, electronic and magnetic) as a function of temperature. The gray horizontal line indicates the configurational entropy S^{conf}. Within the investigated temperature range from 0 to 1200 K, S^{el} and S^{mag} can be significant—up to 0.8 k_B which is about one half of S^{conf}—and are thus non negligible in determining phase stabilities. We observe also that the vibrational entropy S^{vib} quickly rises with temperature reaching values of up to 8 k_B which are five times larger than S^{conf} at 1200 K. These absolute values are however not significant for determining relative phase stabilities, because all phases acquire the same high vibrational entropy value as is visible from Fig. 4 and as it also applies in general for other phases (e.g., intermetallic phases). It is rather the spread in S^{vib} among the different phases which is relevant for relative stabilities and this spread is seen to be in the range 1 k_B, i.e., in a similar order of magnitude as for S^{el} and S^{mag}. Thus, for the investigated HEA alloy we can conclude that entropic contributions beyond the configurational one are non-negligible in determining phase stabilities and can reach values of up to 50% of the configurational entropy.

The electronic entropy contributions for the different crystal structures at different magnetic states can be quite different. Since the electronic density of states (DOS) at the Fermi level, E_F, is the most dominant factor in determining S^{el}, such differences can be typically traced back by investigating the volume dependence of the DOS at E_F. As already discussed above, the bcc structure is the most sensitive one with respect to the considered magnetic state. As shown in Fig. 5, the electronic DOS of bcc also strongly depends on the magnetic state. Consistent with the impact of the magnetic state on the various ground-state properties (discussed in the preceding sections) we further find that the electronic DOS of hcp is not very much dependent on the magnetic state and that the electronic DOS of fcc slightly depends on the magnetic state as the volume increases.

Considering S^{mag}, the contribution is largest for bcc, and lowest for hcp, consistent with the computed local magnetic moments in DLM (see Fig. 1(c)). Below 520 K, S^{mag} in DLM hcp is negligible. The underlying reason are the virtually vanishing moments in the hcp structure. Even at elevated temperatures, the increase in volume is not large enough to allow noticeable formation of local magnetic moments and magnetic entropy (see Fig. 1(c)).

3.4. Comparison with experiments

The thermal expansion of CoCrFeMnNi has been recently measured from 300 to 1270 K [28]. In addition the polycrystalline Young's modulus, E, as well as the shear modulus, G, of the investigated HEA have been measured in Refs. [28,62] within the temperature range from 55 up to 1000 K. If isotropic elasticity is assumed, the bulk modulus is related to E and G via

$$B = \frac{EG}{3(3G - E)}. \tag{12}$$

In order to compare our results with the experimental data, a parametrization of E and G according to Ref. [28] has been employed, i.e.,

$$E = 214\,\text{GPa} - \frac{35\,\text{GPa}}{\exp\left(\frac{416\,\text{K}}{T} - 1\right)}, \tag{13}$$

$$G = 85\,\text{GPa} - \frac{16\,\text{GPa}}{\exp\left(\frac{448\,\text{K}}{T} - 1\right)}. \tag{14}$$
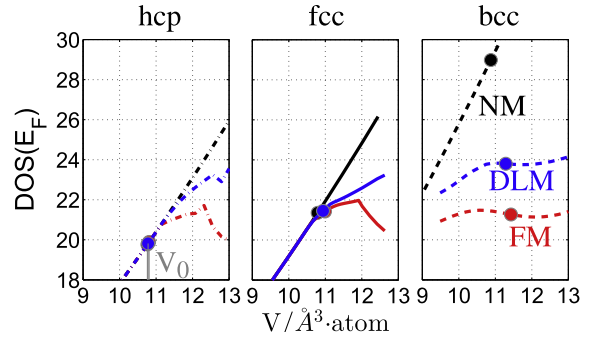

Fig. 5. Electronic density of states (DOS) at the Fermi level, E_F, as a function of the atomic volume, V, in the hcp (left), fcc (middle), and bcc (right) structure. The black lines correspond to the NM (non-magnetic), the red lines to the FM (ferromagnetic), and the blue lines to the DLM (disordered magnetic moment) state. The filled circles indicate where the ground state equilibrium volume of the corresponding crystal structure is.
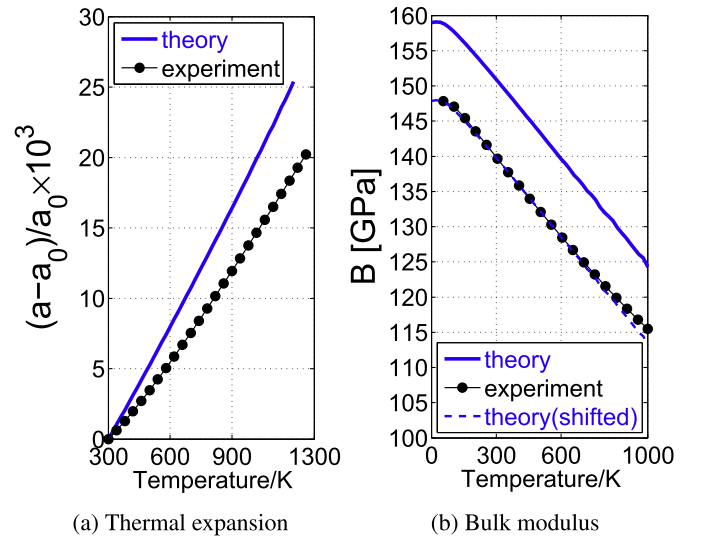

(a) Thermal expansion   (b) Bulk modulus

Fig. 6. Calculated (solid blue lines) (a) thermal expansion and (b) isothermal bulk modulus as a function of temperature compared to experiment (black solid circles) [28,62]. The calculated thermal expansion and bulk modulus correspond to the fcc DLM phase and include all free energy contributions, i.e., electronic, vibrational, and magnetic. The dashed blue line in (b) is obtained by a constant shift of the calculated bulk modulus (blue solid line) to match the experimental bulk modulus extrapolated to $T = 0$ K.

The comparison between calculated and measured relative thermal expansion and bulk modulus as a function of temperature is shown in Fig. 6.

Fig. 6(a) reveals that the temperature dependence of the thermal expansion is overestimated by our calculation. This overestimation is probably a consequence of the employed approximations for the vibrational (Debye–Grüneisen model, see Section 2.1) and magnetic contributions (mean-field approximation, see Section 2.2). Due to the neglect of magnetic short-range order within the latter, the magnetic free energy expression (Eq. (9)) becomes very sensitive to changes in the local magnetic moments. As they strongly increase with increasing volume, the magnetic contribution favors larger equilibrium volumes and hence significantly contributes to the thermal expansion. Consequently, the here computed magnetic contribution to the thermal expansion provides likely an upper limit.

The bulk modulus is likewise overestimated, by about 10 GPa as shown in Fig. 6(b). To investigate the temperature dependence we shift the theoretically predicted bulk modulus so that it agrees

with experiment at low temperatures (dashed blue line in Fig. 6 (b)). The good agreement of the shifted bulk modulus over the whole temperature range reveals the overall good performance of our approach. Only at high temperatures i.e., approximately above 800 K, the calculated bulk modulus is slightly lower than the experiment consistent with the overestimated thermal expansion.

No indications for a phase transition in the temperature range from 55 to 1000 K are observed in the measured polycrystalline Young's modulus and the shear modulus [28,62]. This is an indication that indeed no magnetic transition occurs in the considered temperature range, consistent with our predicted $T_C \approx 20$ K.

4. Conclusions

A finite-temperature *ab initio* method has been applied to compute the electronic, vibrational, and magnetic free energy contributions for a five-component prototype high entropy alloy CoCrFeMnNi. Thermodynamic properties, phase stabilities, and the role of different entropy contributions for different crystal structures (fcc, hcp, and bcc) have been extracted and analyzed. Consistent with experiment the paramagnetic fcc structure was predicted to be the most stable phase at temperatures above room temperature.

Our analysis has revealed that entropy contributions beyond the configurational one are important for determining phase stabilities and other properties of HEA materials. Electronic and magnetic entropies can contribute up to 50% of the configurational entropy value. Since these entropy contributions depend strongly on the electronic density of states at the Fermi level and the local magnetic moments, a variation of these quantities among the various phases causes a strong spread in the corresponding entropy contributions and thus affects phase stability differences significantly.

The vibrational entropy rises quickly in absolute value with temperature up to four times the configurational entropy value. However, since all phases acquire a similar magnitude in vibrational entropy it is thus only the spread in this entropy contribution that can lead to differences among different phases. This spread is similar to the spread in electronic and magnetic entropies and thus all these entropy contributions beyond the configurational one are crucial in determining phase stabilities and should be critically assessed when studying novel HEAs.

In conclusion, our results unveil that the original assumption in the design of HEA material systems—which singles out the configurational entropy as the dominating finite temperature stabilization mechanism—may fail. Vibrational, electronic, and magnetic entropy contributions must be considered on a similar footing. Taking these contributions into account is likely to open new directions in the design of HEA material systems.

References

[1] J.W. Yeh, Alloy design strategies and future trends in high-entropy alloys, JOM 65 (12) (2013) 1759–1771, http://dx.doi.org/10.1007/s11837-013-0761-6. URL: http://link.springer.com/10.1007/s11837-013-0761-6.

[2] Y. Zhang, T.T. Zuo, Z. Tang, M.C. Gao, K.A. Dahmen, P.K. Liaw, et al., Microstructures and properties of high-entropy alloys, Prog. Mater Sci. 2014 (61) (October 2013) 1–93, http://dx.doi.org/10.1016/j.pmatsci.2013.10.001. URL: http://linkinghub.elsevier.com/retrieve/pii/S0079642513000789.

[3] M.H. Tsai, J.W. Yeh, High-entropy alloys: a critical review, Mater. Res. Lett. 2 (3) (2014) 107–123, http://dx.doi.org/10.1080/21663831.2014.912690. URL: http://www.tandfonline.com/doi/abs/10.1080/21663831.2014.912690.

[4] K.Y. Tsai, M.H. Tsai, J.W. Yeh, Sluggish diffusion in CoCrFeMnNi high-entropy alloys, Acta Mater. 61 (13) (2013) 4887–4897, http://dx.doi.org/10.1016/j.actamat.2013.04.058. URL: http://linkinghub.elsevier.com/retrieve/pii/S1359645413003431.

[5] F. Otto, Y. Yang, H. Bei, E. George, Relative effects of enthalpy and entropy on the phase stability of equiatomic high-entropy alloys, Acta Mater. 61 (7) (2013) 2628–2638, http://dx.doi.org/10.1016/j.actamat.2013.01.042. URL: http://linkinghub.elsevier.com/retrieve/pii/S1359645413000694.

[6] A.J.B. Vincent (BSc Part II thesis), A study of three multicomponent alloys, University of Sussex, 1981.

[7] P. Knight (BSc Part II thesis), Multicomponent alloys, University of Oxford, Oxford, UK, 1995.

[8] B. Cantor, I. Chang, P. Knight, A. Vincent, Microstructural development in equiatomic multicomponent alloys, Mater. Sci. Eng.: A 375–377 (2004) 213–218, http://dx.doi.org/10.1016/j.msea.2003.10.257. URL: http://linkinghub.elsevier.com/retrieve/pii/S0921509303009936.

[9] B. Cantor, Stable and metastable multicomponent alloys, Annales de Chimie – Science des Matériaux 32 (3) (2007) 245–256, http://dx.doi.org/10.3166/acsm.32.245-256. URL: http://acsm.revueonline.com/article.jsp?articleId=9708.

[10] B. Cantor, Multicomponent and high entropy alloys, Entropy 16 (9) (2014) 4749–4768, http://dx.doi.org/10.3390/e16094749. URL: http://www.mdpi.com/1099-4300/16/9/4749/.

[11] B. Grabowski, T. Hickel, J. Neugebauer, Ab initio study of the thermodynamic properties of nonmagnetic elementary fcc metals: exchange-correlation-related error bars and chemical trends, Phys. Rev. B 76 (2) (2007) 024309, http://dx.doi.org/10.1103/PhysRevB.76.024309. URL: http://prb.aps.org/abstract/PRB/v76/i2/e024309.

[12] F. Körmann, A. Dick, B. Grabowski, B. Hallstedt, T. Hickel, J. Neugebauer, Free energy of bcc iron: integrated ab initio derivation of vibrational, electronic, and magnetic contributions, Phys. Rev. B 78 (3) (2008) 033102, http://dx.doi.org/10.1103/PhysRevB.78.033102. URL: http://prb.aps.org/abstract/PRB/v78/i3/e033102.

[13] F. Birch, The effect of pressure upon the elastic parameters of isotropic solids, according to Murnaghan's theory of finite strain, J. Appl. Phys. 9 (4) (1938) 279–288, http://dx.doi.org/10.1063/1.1710417. URL: http://link.aip.org/link/?JAP/9/279/1.

[14] F. Birch, Finite elastic strain of cubic crystals, Phys. Rev. 71 (11) (1947) 809–824, http://dx.doi.org/10.1103/PhysRev.71.809. URL: http://prola.aps.org/abstract/PR/v71/i11/p809_1.

[15] B. Grabowski, P. Söderlind, T. Hickel, J. Neugebauer, Temperature-driven phase transitions from first principles including all relevant excitations: the fcc-to-bcc transition in Ca, Phys. Rev. B 84 (2011) 214107, http://dx.doi.org/10.1103/PhysRevB.84.214107. URL: http://link.aps.org/doi/10.1103/PhysRevB.84.214107.

[16] F. Körmann, A. Dick, B. Grabowski, T. Hickel, J. Neugebauer, Atomic forces at finite magnetic temperatures: phonons in paramagnetic iron, Phys. Rev. B 85 (2012) 125104, http://dx.doi.org/10.1103/PhysRevB.85.125104. URL: http://link.aps.org/doi/10.1103/PhysRevB.85.125104.

[17] F. Körmann, B. Grabowski, B. Dutta, T. Hickel, L. Mauger, B. Fultz, et al., Temperature dependent magnon–phonon coupling in bcc Fe from theory and experiment, Phys. Rev. Lett. 113 (2014) 165503, http://dx.doi.org/10.1103/PhysRevLett.113.165503. URL: http://link.aps.org/doi/10.1103/PhysRevLett.113.165503.

[18] L. Zhou, F. Körmann, D. Holec, M. Bartosik, B. Grabowski, J. Neugebauer, et al., Structural stability and thermodynamics of CrN magnetic phases from ab initio calculations and experiment, Phys. Rev. B 90 (2014) 184102, http://dx.doi.org/10.1103/PhysRevB.90.184102. URL: http://link.aps.org/doi/10.1103/PhysRevB.90.184102.

[19] Y. Ikeda, F. Körmann, A. Seko, A. Togo, J. Neugebauer, I. Tanaka, 2015, in preparation.

[20] B. Grabowski, L. Ismer, T. Hickel, J. Neugebauer, Ab initio up to the melting point: anharmonicity and vacancies in aluminum, Phys. Rev. B 79 (13) (2009) 134106, http://dx.doi.org/10.1103/PhysRevB.79.134106. URL: http://prb.aps.org/abstract/PRB/v79/i13/e134106.

[21] A. Glensk, B. Grabowski, T. Hickel, J. Neugebauer, Understanding anharmonicity in fcc materials: from its origin to ab initio strategies beyond the quasiharmonic approximation, Phys. Rev. Lett. 114 (2015) 195901, http://dx.doi.org/10.1103/PhysRevLett.114.195901. URL: http://link.aps.org/doi/10.1103/PhysRevLett.114.195901.

[22] V.L. Moruzzi, J.F. Janak, K. Schwarz, Calculated thermal properties of metals, Phys. Rev. B 37 (1988) 790–799, http://dx.doi.org/10.1103/PhysRevB.37.790. URL: http://link.aps.org/doi/10.1103/PhysRevB.37.790.

[23] H.C. Herper, E. Hoffmann, P. Entel, Ab initio full-potential study of the structural and magnetic phase stability of iron, Phys. Rev. B 60 (1999) 3839–3848, http://dx.doi.org/10.1103/PhysRevB.60.3839. URL: http://link.aps.org/doi/10.1103/PhysRevB.60.3839.

[24] J.C. Slater, Introduction to Chemical Physics, McGraw-Hill Book Company, Inc, New York and London, 1939.

[25] J.S. Dugdale, D.K.C. MacDonald, The thermal expansion of solids, Phys. Rev. 89 (1953) 832–834, http://dx.doi.org/10.1103/PhysRev.89.832. URL: http://link.aps.org/doi/10.1103/PhysRev.89.832.

[26] F. Körmann, A.A.H. Breidi, S.L. Dudarev, N. Dupin, G. Ghosh, T. Hickel, et al., Lambda transitions in materials science: recent advances in CALPHAD and first-principles modelling, Phys. Status Solidi (b) 251 (1) (2014) 53–80, http://dx.doi.org/10.1002/pssb.201350136.

[27] F. Körmann, T. Hickel, J. Neugebauer, Influence of magnetic excitations on the phase stability of metals and steels, Curr. Opin. Solid State Mater. Sci. (2015). in press, URL: http://www.sciencedirect.com/science/article/pii/S1359028615300012.

[28] G. Laplanche, P. Gadaud, O. Horst, F. Otto, G. Eggeler, E. George, Temperature dependencies of the elastic moduli and thermal expansion coefficient of an equiatomic, single-phase CoCrFeMnNi high-entropy alloy, J. Alloy. Compd. 623 (0) (2015) 348–353, http://dx.doi.org/10.1016/j.jallcom.2014.11.061. URL: http://www.sciencedirect.com/science/article/pii/S0925838814027042.

[29] Inden G. In, Proc. Calphad (1976) 1–13.

[30] K. Sato, H. Katayama-Yoshida, P. Dederichs, Diluted magnetic semiconductors, Ψ_k Newsletter (70) (2005) 93–110. URL: http://www.psi-k.org/newsletters/News_70/Highlight_70.pdf; scientific highlight of the month.

[31] F. Körmann, A. Dick, T. Hickel, J. Neugebauer, Pressure dependence of the Curie temperature in bcc iron studied by ab initio simulations, Phys. Rev. B 79 (2009) 184406, http://dx.doi.org/10.1103/PhysRevB.79.184406. URL: http://link.aps.org/doi/10.1103/PhysRevB.79.184406.

[32] L. Vitos, H. Skriver, B. Johansson, J. Kollár, Application of the exact muffin-tin orbitals theory: the spherical cell approximation, Comput. Mater. Sci. 18 (1) (2000) 24–38, http://dx.doi.org/10.1016/S0927-0256(99)00098-1. URL: http://www.sciencedirect.com/science/article/pii/S0927025699000981.

[33] L. Vitos, Total-energy method based on the exact muffin-tin orbitals theory, Phys. Rev. B 64 (2001) 014107, http://dx.doi.org/10.1103/PhysRevB.64.014107. URL: http://link.aps.org/doi/10.1103/PhysRevB.64.014107.

[34] L. Vitos, I.A. Abrikosov, B. Johansson, Anisotropic lattice distortions in random alloys from first-principles theory, Phys. Rev. Lett. 87 (2001) 156401, http://dx.doi.org/10.1103/PhysRevLett.87.156401. URL: http://link.aps.org/doi/10.1103/PhysRevLett.87.156401.

[35] L. Vitos, Computational Quantum Mechanics for Materials Engineers, Springer, London, 2007, http://dx.doi.org/10.1007/978-1-84628-951-4.

[36] P. Hohenberg, W. Kohn, Inhomogeneous electron gas, Phys. Rev. 136 (1964) B864–B871, http://dx.doi.org/10.1103/PhysRev.136.B864. URL: http://link.aps.org/doi/10.1103/PhysRev.136.B864.

[37] W. Kohn, L.J. Sham, Self-consistent equations including exchange and correlation effects, Phys. Rev. 140 (4A) (1965) A1133–A1138, http://dx.doi.org/10.1103/PhysRev.140.A1133. URL: http://prola.aps.org/abstract/PR/v140/i4A/pA1133_1.

[38] P. Soven, Coherent-potential model of substitutional disordered alloys, Phys. Rev. 156 (1967) 809–813, http://dx.doi.org/10.1103/PhysRev.156.809. URL: http://link.aps.org/doi/10.1103/PhysRev.156.809.

[39] B.L. Gyorffy, Coherent-potential approximation for a nonoverlapping-muffin-tin-potential model of random substitutional alloys, Phys. Rev. B 5 (1972) 2382–2384, http://dx.doi.org/10.1103/PhysRevB.5.2382. URL: http://link.aps.org/doi/10.1103/PhysRevB.5.2382.

[40] A.V. Ruban, H.L. Skriver, Screened Coulomb interactions in metallic alloys. I. Universal screening in the atomic-sphere approximation, Phys. Rev. B 66 (2002) 024201, http://dx.doi.org/10.1103/PhysRevB.66.024201. URL: http://journals.aps.org/prb/abstract/10.1103/PhysRevB.66.0242010.

[41] A.V. Ruban, S.I. Simak, P.A. Korzhavyi, H.L. Skriver, Screened Coulomb interactions in metallic alloys. II. Screening beyond the single-site and atomic-sphere approximations, Phys. Rev. B 66 (2002) 024202, http://dx.doi.org/10.1103/PhysRevB.66.024202. URL: http://journals.aps.org/prb/abstract/10.1103/PhysRevB.66.024202.

[42] J.P. Perdew, K. Burke, M. Ernzerhof, Generalized gradient approximation made simple, Phys. Rev. Lett. 77 (1996) 3865–3868, http://dx.doi.org/10.1103/PhysRevLett.77.3865. URL: http://link.aps.org/doi/10.1103/PhysRevLett.77.3865.

[43] H.J. Monkhorst, J.D. Pack, Special points for brillouin-zone integrations, Phys. Rev. B 13 (1976) 5188–5192, http://dx.doi.org/10.1103/PhysRevB.13.5188. URL: http://link.aps.org/doi/10.1103/PhysRevB.13.5188.

[44] J. Staunton, B. Gyorffy, A. Pindor, G. Stocks, H. Winter, The disordered local moment picture of itinerant magnetism at finite temperatures, J. Magn. Magn. Mater. 45 (1) (1984) 15–22, http://dx.doi.org/10.1016/0304-8853(84)90367-6. URL: http://www.sciencedirect.com/science/article/pii/0304885384903676.

[45] B.L. Gyorffy, A.J. Pindor, J. Staunton, G.M. Stocks, H. Winter, A first-principles theory of ferromagnetic phase transitions in metals, J. Phys. F: Met. Phys. 15 (6) (1985) 1337, http://dx.doi.org/10.1088/0305-4608/15/6/018. URL: http://stacks.iop.org/0305-4608/15/i=6/a=018.

[46] F. Tian, L. Varga, N. Chen, L. Delczeg, L. Vitos, Ab initio investigation of high-entropy alloys of 3d elements, Phys. Rev. B 87 (7) (2013) 075144, http://dx.doi.org/10.1103/PhysRevB.87.075144. URL: http://link.aps.org/doi/10.1103/PhysRevB.87.075144.

[47] F. Tian, L. Delczeg, N. Chen, L.K. Varga, J. Shen, L. Vitos, Structural stability of NiCoFeCrAl$_x$ high-entropy alloy from ab initio theory, Phys. Rev. B 88 (8) (2013) 085128, http://dx.doi.org/10.1103/PhysRevB.88.085128. URL: http://link.aps.org/doi/10.1103/PhysRevB.88.085128.

[48] F. Tian, L.K. Varga, N. Chen, J. Shen, L. Vitos, Ab initio design of elastically isotropic TiZrNbMoV$_x$ high-entropy alloys, J. Alloy. Compd. 599 (14) (2014) 19–25, http://dx.doi.org/10.1016/j.jallcom.2014.01.237. URL: http://linkinghub.elsevier.com/retrieve/pii/S0925838814003089.

[49] E. Fazakas, V. Zadorozhnyy, L. Varga, A. Inoue, D. Louzguine-Luzgin, F. Tian, et al., Experimental and theoretical study of Ti$_{20}$Zr$_{20}$Hf$_{20}$Nb$_{20}$X$_{20}$ (X=V or Cr) refractory high-entropy alloys, Int. J. Refract. Met. Hard Mater. 47 (2014) 131–138, http://dx.doi.org/10.1016/j.ijrmhm.2014.07.009. URL: http://linkinghub.elsevier.com/retrieve/pii/S0263436814001516.

[50] P. Cao, X. Ni, F. Tian, L.K. Varga, L. Vitos, Ab initio study of AlxMoNbTiV high-entropy alloys, J. Phys.: Condens. Matter 27 (7) (2015) 075401, http://dx.doi.org/10.1088/0953-8984/27/7/075401. URL: http://iopscience.iop.org/0953-8984/27/7/075401.

[51] T. Gebhardt, D. Music, B. Hallstedt, M. Ekholm, I.A. Abrikosov, L. Vitos, et al., Ab initio lattice stability of fcc and hcp Fe–Mn random alloys, J. Phys.: Condens. Matter 22 (29) (2010) 295402, http://dx.doi.org/10.1088/0953-8984/22/29/295402. URL: http://stacks.iop.org/0953-8984/22/i=29/a=295402.

[52] C. Niu, A.J. Zaddach, A.A. Oni, X. Sang, J.W. Hurt, J.M. LeBeau, et al., Spin-driven ordering of Cr in the equiatomic high entropy alloy NiFeCrCo, Appl. Phys. Lett. 106 (16) (2015) 161906, http://dx.doi.org/10.1063/1.4918996. URL: http://scitation.aip.org/content/aip/journal/apl/106/16/10.1063/1.4918996.

[53] F. Otto, A. Dlouhý, C. Somsen, H. Bei, G. Eggeler, E. George, The influences of temperature and microstructure on the tensile properties of a CoCrFeMnNi high-entropy alloy, Acta Mater. 61 (15) (2013) 5743–5755, http://dx.doi.org/10.1016/j.actamat.2013.06.018. URL: http://linkinghub.elsevier.com/retrieve/pii/S1359645413004503.

[54] Y. Wu, W.H. Liu, X.L. Wang, D. Ma, A.D. Stoica, T.G. Nieh, et al., In-situ neutron diffraction study of deformation behavior of a multi-component high-entropy alloy, Appl. Phys. Lett. 104 (5) (2014) 051910, http://dx.doi.org/10.1063/1.4863748. URL: http://scitation.aip.org/content/aip/journal/apl/104/5/10.1063/1.4863748.

[55] B. Gludovatz, A. Hohenwarter, D. Catoor, E.H. Chang, E.P. George, R.O. Ritchie, A fracture-resistant high-entropy alloy for cryogenic applications, Science 345 (6201) (2014) 1153–1158, http://dx.doi.org/10.1126/science.1254581. URL: http://www.sciencemag.org/cgi/doi/10.1126/science.1254581.

[56] N. Stepanov, M. Tikhonovsky, N. Yurchenko, D. Zyabkin, M. Klimova, S. Zherebtsov, et al., Effect of cryo-deformation on structure and properties of CoCrFeNiMn high-entropy alloy, Intermetallics 59 (0) (2015) 8–17, http://dx.doi.org/10.1016/j.intermet.2014.12.004. URL: http://www.sciencedirect.com/science/article/pii/S0966979514003082.

[57] S. Kibey, J. Liu, M. Curtis, D. Johnson, H. Sehitoglu, Effect of nitrogen on generalized stacking fault energy and stacking fault widths in high nitrogen steels, Acta Mater. 54 (11) (2006) 2991–3001, http://dx.doi.org/10.1016/j.actamat.2006.02.048. URL: http://www.sciencedirect.com/science/article/B6TW8-4JYKM1S-2/2/1a525ad29b77d8efcfe88ef192295bf5.

[58] F. Zhang, C. Zhang, S. Chen, J. Zhu, W. Cao, U. Kattner, An understanding of high entropy alloys from phase diagram calculations, Calphad 45 (2014) 1–10, http://dx.doi.org/10.1016/j.calphad.2013.10.006. URL: http://linkinghub.elsevier.com/retrieve/pii/S0364591613001028.

[59] M. Laurent-Brocq, A. Akhatova, L. Perrière, S. Chebini, X. Sauvage, E. Leroy, et al., Insights into the phase diagram of the CrMnFeCoNi high entropy alloy, Acta Mater. 88 (2015) 355–365, http://dx.doi.org/10.1016/j.actamat.2015.01.068. URL: http://www.sciencedirect.com/science/article/pii/S1359645415000088.

[60] B. Schuh, F. Mendez-Martin, B. Völkera, E.P. George, H. Clemens, R. Pippan, A. Hohenwarter, Mechanical properties, microstructure and thermal stability of a nanocrystalline CoCrFeMnNi high-entropy alloy after severe plastic deformation, Acta Mater. 96 (2015) 258–268, http://dx.doi.org/10.1016/j.actamat.2015.06.025. URL: http://www.sciencedirect.com/science/article/pii/S1359645415004115.

[61] D. Ma, M. Yao, K.G. Pradeep, C.C. Tasan, H. Springer, D. Raabe, Phase stability of non-equiatomic CoCrFeMnNi high entropy alloys, Acta Mater. 98 (2015) 288–296, http://dx.doi.org/10.1016/j.actamat.2015.07.030. URL: http://www.sciencedirect.com/science/article/pii/S1359645415005017.

[62] A. Haglund, M. Koehler, D. Catoor, E. George, V. Keppens, Polycrystalline elastic moduli of a high-entropy alloy at cryogenic temperatures, Intermetallics 58 (0) (2015) 62–64, http://dx.doi.org/10.1016/j.intermet.2014.11.005. URL: http://www.sciencedirect.com/science/article/pii/S0966979514002982.